Image Distortion Correction in EPI: Comparison of Field Mapping With Point Spread Function Mapping

Huairen Zeng[1] and R. Todd Constable[1,2*]

Echo-planar imaging (EPI) can provide rapid imaging by acquiring a complete *k*-space data set in a single acquisition. However, this approach suffers from distortion effects in geometry and intensity, resulting in poor image quality. The distortions, caused primarily by field inhomogeneities, lead to intensity loss and voxel shifts, the latter of which are particularly severe in the phase-encode direction. Two promising approaches to correct the distortion in EPI are field mapping and point spread function (PSF) mapping. The field mapping method measures the field distortions and translates these into voxel shifts, which can be used to assign image intensities to the correct voxel locations. The PSF approach uses acquisitions with additional phase-encoding gradients applied in the *x*, *y*, and/or *z* directions to map the 1D, 2D, or 3D PSF of each voxel. These PSFs encode the spatial information about the distortion and the overall distribution of intensities from a single voxel. The measured image is the convolution of the undistorted density and the PSF. Measuring the PSF allows the distortion in geometry and intensity to be corrected. This work compares the efficacy of these methods with equal time allowed for field mapping and PSF mapping. Magn Reson Med 48:137–146, 2002. © 2002 Wiley-Liss, Inc.

Key words: echo-planar imaging; point spread function; field mapping; geometric distortion; rapid imaging

Echo planar imaging (EPI) is commonly used in applications such as functional MRI (fMRI) because of the speed at which it can acquire images. However, the long echo readout time required by EPI, combined with the typically large internal magnetic field inhomogeneities caused by susceptibility differences at tissue/air and tissue/bone interfaces, results in significant geometric and intensity distortions in single-shot EPI images. The challenge of reducing these field inhomogeneity effects arises from their spatial dependence. Data from different spatial locations are corrupted to different degrees, with the amount of corruption determined by the local magnetic field environment. The measured *k*-space data is the supposition of *k*-space data from individual voxels, and since each voxel potentially requires a different correction term, applying a single correction term to the complete *k*-space data is not very effective.

Single reference scans (1), acquired by turning off the blipped phase-encoding gradients of the EPI sequence, can reduce the N/2 ghosting. These reference scans measure the position shift in *k*-space caused by the field inhomogeneities, and these shifts, which are dependent upon the polarity of the readout gradient, are easily corrected with a reference scan. However, because the field inhomogeneity is position-dependent, and hence the resultant phase errors are position-dependent, a single reference scan approach cannot correct the distortion caused by field inhomogeneity. Xin et al. (2) proposed an approach incorporating a scan that uses multiple references rather than a single reference. In the multi-reference scan method, during the i^{th} reference scan, $[i - 1]$ phase-encoding blips are played out before the readout gradient so that all the data from the i^{th} excitation is phase-encoded equally. To correct the distortion, a filter is computed from these multi-reference scans, and is applied directly to the EPI *k*-space. This approach appears to be effective as long as the assumption that the spatial distribution of the field inhomogeneity is slowly varying is satisfied, which is usually the case.

Another multi-reference technique, proposed by Chen et al. (3), incorporates a single phase-encode gradient before each echo, such that all the echoes are phase-encoded equally. The phase-encode gradient varies in each repeated scan to fully cover the k_y space. The first echo image is then obtained from the first echo of all the repeated scans, and the n^{th} echo image is obtained from the n^{th} echo. In *k*-space, the difference between the first echo image and n^{th} echo image is that the latter has an additional phase, which accumulates during the time interval $n\Delta T$, and arises from field inhomogeneity and chemical shift effects. Distortion is not a problem in this case because the same phase accumulation is present for all of *k*-space for the n^{th} echo image, just as in conventional (non-EPI) imaging sequences. However, each image has a different phase shift associated with it, and thus a phase modulation function can be obtained which can then be applied to subsequent distorted EPI acquisitions. In *k*-space, phase modulating the distorted EPI images with a modulation factor that is the complex ratio of the n^{th} echo image to the first echo image, and then Fourier transforming this modulated *k*-space image, yields the undistorted EPI image. The advantage of this approach is that it avoids the phase wrap problem, as occurs in the field mapping approach discussed below. The disadvantage of both of the multi-reference scan approaches described above is that they require longer scan times. For a data acquisition matrix size of $N_x \times N_y$, N_y repeated scans are required.

Kadah and Hu (4) proposed a method that uses a distortion kernel to undo or rewind the additional phase accumulated from the field inhomogeneities. The distortion kernel is calculated using an initial estimate of the image and a field map derived from two segmented EPI images

[1]Department of Diagnostic Radiology, Yale University School of Medicine, New Haven, Connecticut.

[2]Department of Neurosurgery, Yale University School of Medicine, New Haven, Connecticut.

Grant sponsor: NIH; Grant numbers: NS-40497; R01 NS-38467.

*Correspondence to: R. Todd Constable, Yale University School of Medicine, Department of Diagnostic Radiology, 333 Cedar St., P.O. Box 208042, New Haven, CT 06520-8042. E-mail: todd.constable@yale.edu

Received 14 August 2001; revised 20 February 2002; accepted 25 February 2002.

DOI 10.1002/mrm.10200

Published online in Wiley InterScience (www.interscience.wiley.com).

collected at different echo times (TEs). This method works if the field inhomogeneity is small and changes smoothly, and if the initial estimate of the image is adequate; if not, the method fails.

An alternative approach uses the information obtained in the image space to determine the pixel shift and reconstruct an undistorted image. This swapped phase and frequency axis approach (5) uses two magnitude images obtained with orthogonal phase-encoding directions. The pixel shift in the phase direction in these two images may be written as $\Delta r(x, y') = y' - y$, and $\Delta r(x', y) = x' - x$. Expanding Δr in a power series up to second order, and minimizing the square difference, $[\rho_1(x,y') - \rho_2(x',y)]2$, the pixel shift Δr can be obtained, thus correcting the distortion. This method requires good initial values for expression of Δr, and becomes less effective as the severity of the local field gradient increases. For computational simplicity, higher-order Taylor series are ignored, and the low-order terms are sufficient for the weak local field gradient. For strong local gradient fields, such as those found in the basal temporal regions of the brain, a high-order Taylor series is required, which increases the complexity of the calculation. A similar approach is to acquire two images with opposite increments in the phase-encoding gradient (6), thereby reversing the distortion in the phase-encoding direction between the two acquisitions. As in the orthogonal phase-encoding direction approach, the magnitude images may be used to construct an undistorted image. In both of these approaches spatial overlap of voxels leads to problems because of the violation of the one-to-one assumption in transformation between the distorted and undistorted space. These approaches also suffer in the lower signal area, where the noise may dominate.

Two other techniques are the field map approach (7–9) and the point spread function (PSF) approach (10). The field map approach has significant potential to provide robust correction of distorted images. In this method changes in the local magnetic field are mapped, and these changes can be directly related to pixel shifts in the image. The limitations of field mapping arise from the difficulty of calculating the phase maps near edges or in regions of high-field inhomogeneity, the problem of phase unwrapping, and the lack of information on voxel intensity. Despite these problems, field mapping has been shown to be quite effective at reducing image distortions (8,9). The PSF approach (10) has the potential to provide robust solutions to the distortion problem in regions of high- or low-field inhomogeneity, and to allow for correction of both geometric and intensity distortions whether or not the voxels are overlapping in the distorted image. It is computationally more involved than the field map correction approach, but potentially provides a better solution. This work further develops the PSF approach and evaluates its performance relative to the field mapping method, with the constraint that the acquisition times for the field mapping and PSF mapping are equal.

THEORY OF GEOMETRIC DISTORTION IN EPI

In conventional single-shot EPI, all the lines of k-space are acquired in a raster scan trajectory after a single RF excitation. The components of k_x and k_y are given by (11,12)

$$k_x(t) = \gamma \int_0^t G_x(t')dt' \quad \text{and} \quad k_y(t) = \gamma \int_0^t G_y(t')dt'. \quad [1]$$

Where γ is the gyromagnetic ratio (2.68×10^8 rad $s^{-1}T^{-1}$) for protons, and $G_x(t)$ and $G_y(t)$ are time-varying gradient fields in the x and y directions. The time t can be expressed as

$$t = TE + nT \pm m\Delta t. \quad [2]$$

Where TE is the echo time, n is the n^{th} k_y line, m is the m^{th} reading point in the x direction, Δt is the dwell time, and T is the time interval between adjacent k_y lines. Let $k_x = m\Delta k_x$, $ky = n\Delta k_y$, with $-N_x/2 \le m_x/2$, $-N_y/2 \le n < N_y/2$, N_x is the number of data points in the readout direction and N_y are the phase-encoding steps. Then the EPI signal can be expressed as

$$S(m\Delta k_x, n\Delta k_y) = \int\int \rho(x,y) e^{-(nT \pm m\Delta t + TE)/T2} e^{i\gamma\Delta B(nT \pm m\Delta t)} e^{i(m\Delta k_x x + n\Delta k_y y)} dxdy. \quad [3]$$

Where $\Delta B(x,y)$ is the magnetic field inhomogeneity, and Δk_x andΔk_y are gradient area increments in the readout and phase-encoding directions, respectively, with

$$\Delta k_x = \frac{2\pi}{Fov_x} = \gamma G_x \Delta t \quad \text{and} \quad \Delta k_y = \frac{2\pi}{Fov_y} = Area_{blip} = \gamma \bar{G}_y \tau \quad [4]$$

where $\bar{G}_y$ is the average area of the phase-encode gradient blip, of duration τ. Ignoring T_2 relaxation, Eq. [3] can be rewritten as:

$$S(m\Delta k_x, n\Delta k_y) = \int\int \rho(x,y) e^{i[m\Delta k_x(x \pm \Delta B/G_x) + n\Delta k_y(y + \Delta BT/\bar{G}_y\tau)]} dxdy \quad [5]$$

or

$$S(k_x,k_y) = \int\int \rho(x,y) e^{i[k_x(x \pm \Delta B/G_x) + k_y(y + \Delta BT/\bar{G}_y\tau)]} dxdy. \quad [6]$$

After Fourier transform of $S(k_x,k_y)$, the measured image density is obtained:

$$\rho_1(x_1,y_1) = \int\int S(k_x,k_y) e^{-1(k_x x_1 + k_y y_1)} dk_x dk_y \quad [7]$$

$$\rho_1(x_1,y_1) = \rho\left(x \pm \frac{\Delta B(x,y)}{G_x},\ y + \frac{\Delta B(x,y)T}{\bar{G}_y\tau} \right). \quad [8]$$

Equation [8] shows that the measured image is distorted due to the field inhomogeneity, with position shifts in x and y defined as:

$$x_1 = x \pm \frac{\Delta B(x,y)}{G_x} \quad \text{and} \quad y_1 = y + \frac{\Delta B(x,y)T}{\bar{G}G_y\tau}. \qquad [9]$$

Equation [9] demonstrates that the largest distortions are in the phase-encoding direction.

FIELD MAP METHOD

Since the field inhomogeneity causes distortion, it should be possible to correct this distortion by measuring the field map. To obtain the field map, an asymmetric spin-echo EPI pulse sequence is used, with a set of time offsets (0, Δt_1, $2\Delta t_1$. . . .$Q\Delta t_1$) between the gradient and spin echoes. The EPI signal for the q^{th} time offset is

$$S(k_x,k_y) = \int\int \rho(x,y)\boldsymbol{e}^{iq\gamma\Delta B(x,y)\Delta t_1}\boldsymbol{e}^{i[k_x(x\pm\Delta B/G_x)+k_y(y+\Delta BT/\bar{G}_y\tau)]}dxdy \qquad [10]$$

and after Fourier transform, the image density is

$$\rho_q(x_1,y_1) = \boldsymbol{e}^{iq\Delta B(x\pm\Delta B(x,y)/G_x,\ y+\Delta B(x,y)T/\bar{G}_y\tau)\Delta t_1} \times \rho\left(x \pm \frac{\Delta B(x,y)}{G_x}, y + \frac{\Delta B(x,y)T}{\bar{G}_y\tau}\right). \qquad [11]$$

The phase for the q^{th} time offset image density is then

$$\Phi_q(x_1,y_1) = i\ q\Delta B\left(x \pm \frac{\Delta B(x,y)}{G_x}, y + \frac{\Delta B(x,y)T}{\bar{G}_y\tau}\right)\Delta t_1 \pm q_1 2\pi. \qquad [12]$$

The last term in Eq. [12] takes into consideration any phase wrap. After phase unwrapping, these Q phases are linear in time; thus, fitting a straight line allows $\Delta B(x,y)$ to be determined from the slope of this line:

$$\phi(x_1, y_1)/\Delta t_1 = \gamma\Delta B(x_1, y_1). \qquad [13]$$

The field map is then combined with the distorted image in order to generate a new data set

$$S(k_x,k_y) = \int\int \rho_1(x_1,y_1)\boldsymbol{e}^{i(k_x(x_1\pm\Delta B/G_x)+k_y(y_1+\Delta BT/\bar{G}_y\tau)]}dx_1dy_1 \qquad [14]$$

such that an approximately correct image is then obtained by Fourier transform of $S(k_x, k_y)$

$$\rho_{correct}(x,y) = \int\int S(k_x,k_y)\boldsymbol{e}^{-i(k_xx+k_yy)}dk_xdk_y \qquad [15]$$

in a manner analogous to the simulated phase evolution rewinding (SPHERE) technique described by Kadah and Hu (4). This is the k-space equivalent of using the field map to reverse pixel shifts in the image space (8).

PSF METHOD

As in the field map method above, the distortion of the MR signal as a function of the field inhomogeneity may be written as

$$S'(\vec{k}') = \int \rho(\vec{r})e^{i\vec{k}\cdot\vec{r}}e^{i\vec{k}\cdot\vec{a}\Delta B(\vec{r})}d\vec{r} \qquad [16]$$

where $\vec{a}$ is a constant vector. If an additional phase-encoding gradient is applied before the collection of an image data set, this will add an additional phase to the data (10). Similar to normal phase encoding for spatial localization, the amplitude of this gradient may be varied according to the local field of view (FOV), thus providing a spatial map of distortion for each individual voxel, just as the normal phase encoding provides the spatial information of the image density. Let $\vec{k}_1$ be the corresponding vector in k-space for this additional gradient. The acquired signal then becomes

$$S'(\vec{k}',\vec{k}_1) = \int \rho(\vec{r})\boldsymbol{e}^{i(\vec{k}' + \vec{k}_1)\ \cdot\ \vec{r}}\boldsymbol{e}^{i\vec{k}'\ \cdot\ \vec{a}\Delta B(\vec{r})}d\vec{r}. \qquad [17]$$

Fourier transforming $S'(\vec{k}, \vec{k}_1)$ with respect to both $\vec{k}'$ and $\vec{k}_1$, using $\vec{r}'$ and $\vec{r}_1$ as conjugate variables,

$$I(\vec{r}',\vec{r}_1) = \int S(\vec{k}',\vec{k}_1)\boldsymbol{e}^{-i\vec{k}'\cdot\vec{r}'}\ \boldsymbol{e}^{-i\vec{k}_1\cdot\vec{r}_1}\ d\vec{k}'d\vec{k}_1 = \rho(\vec{r}_1)\delta[\vec{r}' - \vec{r}_1 - \vec{a}\Delta B(\vec{r}_1)]\ =\ \rho(\vec{r}_1)H(\vec{r},\vec{r}_1) \qquad [18]$$

where

$$H(\vec{r}',\vec{r}) = \int \boldsymbol{e}^{i\vec{k}_1\cdot(\vec{r}'-\vec{r}_1-a\Delta B(\vec{r})}d\vec{k}_1 = \delta[\vec{r}' - \vec{r}_1 - \vec{a}\Delta B(\vec{r})] \qquad [19]$$

and $H(\vec{r}', \vec{r})$ is the PSF (10). The measured image density is

$$I(\vec{r}') = \int \rho(\vec{r})\boldsymbol{e}^{-i\vec{k}\cdot\vec{r}'}\ d\vec{k}' = \int \rho(\vec{r})\delta[\vec{r}' - \vec{r} - \vec{a}\Delta B(\vec{r})]d\vec{r} = \rho[\vec{r}' - \vec{r} - \vec{a}\Delta B(\vec{r})] = \int \rho(\vec{r})H(\vec{r}',\vec{r})d\vec{r}. \qquad [20]$$

Equation [20] shows that the measured image is the convolution of undistorted image with the PSF (10). The resultant distortion from the field inhomogeneity is then $\vec{r}' = \vec{r} + \vec{a}\Delta B(\vec{r})$. As expected, this distortion information is exactly reflected in the PSF shown in Eq. [20]. The undistorted image is determined through deconvolution of the

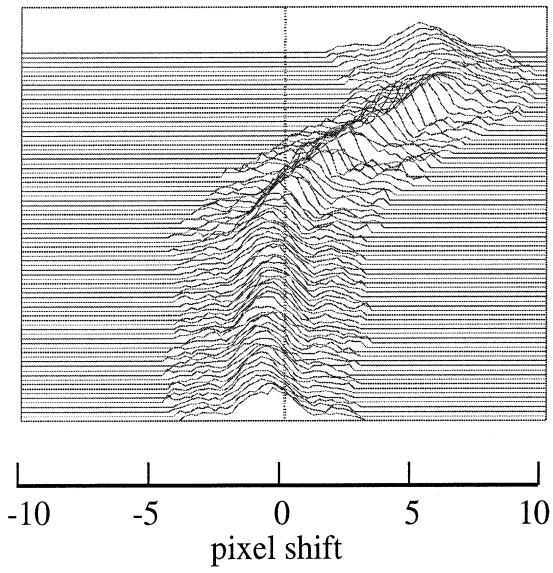

FIG. 1. The PSF for every other voxel along a line in the phase-encode direction for the phantom shown in Fig. 2. The solid vertical line represents the correct position of the voxels if no distortion was present. The image distortion is shown by the shift of the PSFs to the right or left along the *y*-axis. Such PSFs contain information on pixel shifts, pixel intensities, and blurring.

distorted image with the PSF. If Eq. [18] is integrated over the distorted space, we obtain

$$\int I(\vec{r}',\vec{r})d\vec{r}' = \int \rho(\vec{r})\delta[\vec{r}' - \vec{r} - \vec{a}\Delta B(\vec{r})]d\vec{r}' = \rho(\vec{r}) \quad [21]$$

which yields the undistorted image. Using Eqs. [18] and [21], the PSF $H(\vec{r}', \vec{r}_1)$ may be obtained. If there is no distortion, the PSF is centered about zero. Distortion causes the PSF to move away from zero by an amount directly proportional to the pixel shift. Figure 1 shows the PSF for every other voxel along a line in the phase-encode direction through an image of a phantom. The vertical line at $x = 0$ represents the undistorted voxel location, and the PSFs demonstrate distortion along the entire cross section of the phantom. Since the local FOV for the PSF measurement may be chosen to be smaller than the image FOV, it is possible to measure subvoxel pixel shifts with this approach. Integrating the product of the PSF with the measured image yields:

$$\int I(\vec{r}')H(\vec{r}',\vec{r})d\vec{r} = \int \rho(\vec{r}'')\, d\vec{r}'' \int H(\vec{r}',\vec{r}'')\, H(\vec{r}',\vec{r})d\vec{r}. \quad [22]$$

If the PSF is replaced by a delta function with the same shift, the above integration yields the undistorted image, which can be used in Eq. [21] to determine the corrected image.

METHODS

Imaging was performed on a GE Signa 1.5 Tesla magnet. The imaging times for field mapping and PSF mapping were always equal. For both methods, FOV = 24 cm, TE = 60 ms, TR = 600 ms, and matrix size = 128 × 128. For the field mapping, 32 echo offsets with a TE increment between echoes of $\Delta t = 1.0$ ms were used. Since the primary distortion is in the phase-encoding direction, as discussed above, only this direction was considered in this work. As shown in a previous work (10), the PSF can be calculated in all three spatial directions, but only the PSF in the phase-encode direction is measured here (since the imaging time for mapping in multiple dimensions increases as the power of N_{DIM}). The local FOV was chosen to be 6 cm for the PSF measurements, and either 32 or 64 phase-encoding steps were used. The resultant PSFs represent 1D profiles of each voxel in the *y* direction. Both phantoms and human subjects were imaged in the axial and coronal imaging planes. In order to emphasize the distortions and to clearly illustrate the corrections, a 128 × 128 acquisition matrix size was used. For this large matrix size, if a short TE is chosen using single-shot EPI, only partial k_y lines are obtained, and thus it is necessary to use the symmetry property of *k*-space to obtain the missing k_y lines. Because a time offset is used in the field mapping method, the $k_y = 0$ line is no longer at the echo center, and thus the symmetry property cannot be used. Instead, a longer TE (160 ms) is chosen to obtain the field map using a full *k*-space acquisition. This field map can then be applied to acquisitions collected with shorter TEs and partial *k*-space sampling. In all comparisons equal time was allocated for PSF measurements and field mapping. Thus, if 32 phase-encode steps were used to measure the PSF, then 32 different echo offsets were used to measure the field map. In both cases, since EPI is used to acquire the field map and PSF data, these acquisitions can be completed in less than a minute.

RESULTS

Figure 2 shows images of a standard quality-assurance phantom, obtained in the axial plane. In Fig. 2a, a conventional spin-echo image, with no distortion in the phase-encode direction, is shown as a reference image. Figure 2c shows the uncorrected original EPI image (128 × 128), Fig. 2b the image obtained when applying the PSF approach, and Fig. 2d the image obtained using the field map approach. Note the large amount of distortion in the original EPI acquisition with no correction (Fig. 2c). The phase-encode direction is vertical and shows maximal distortion effects, as expected. The correction using the PSF appears to be superior to that obtained using the field mapping approach. The two bright tubes clearly seen in the conventional acquisition (Fig. 2a) are fully recovered in the PSF-corrected EPI image, but are only partially recovered in the field mapping approach. The residual intensity loss in the field map approach is due to in-plane dephasing, which the field mapping method cannot recover.

Figure 3 shows an example of this comparison in axial-oblique images from a normal control subject. Figure 3a shows the conventional spin-echo image used as a reference image. Figure 3c shows the uncorrected EPI image, Fig. 3b shows the PSF-corrected image, and Fig. 3d shows the field map-corrected image. The PSF approach provides

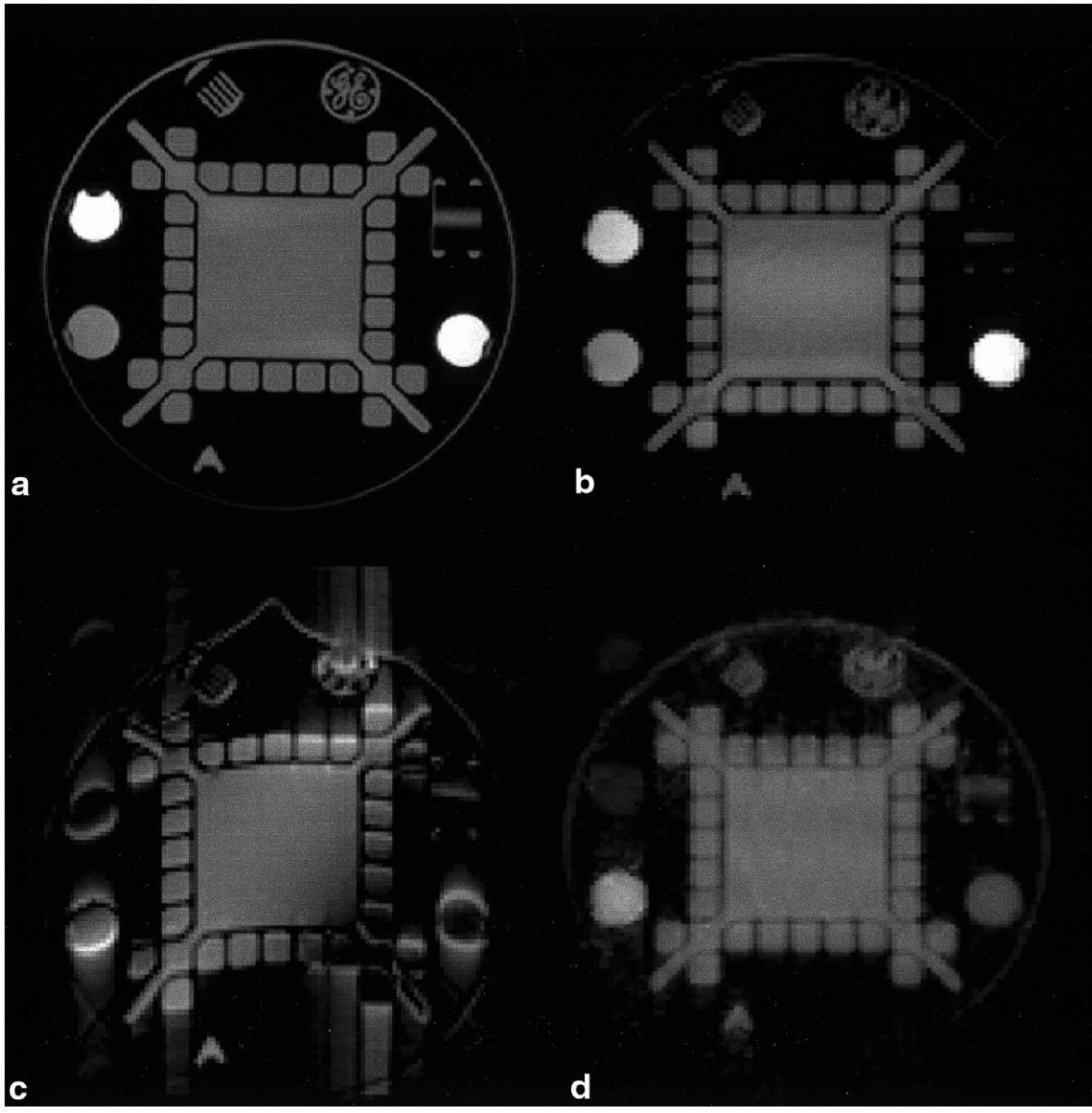

FIG. 2. Phantom images: (**a**) conventional spin-echo image, (**b**) PSF-corrected EPI image, (**c**) uncorrected EPI image, and (**d**) field map-corrected EPI image. The phase-encode direction is vertical.

excellent recovery of signal in regions of maximal distortion (near the auditory canals bilaterally) and is unaffected by the overlapping voxels in this region. In this region of high-field inhomogeneity it is difficult to obtain an accurate field map, and the correct assignment of voxel intensity when these overlapping voxels are separated is also difficult.

Figure 4 shows an example from another normal volunteer, this time with the images obtained in the coronal plane. The conventional spin-echo reference image with no distortion is shown in Fig. 4a. Figure 4b shows the PSF-corrected image, and Fig. 4c the original uncorrected EPI image—the latter again demonstrating significant distortion. The field map-corrected image is shown in Fig. 4d, and demonstrates residual intensity anomalies in regions of high-field inhomogeneity. The increase in noise (Fig. 4d) in areas in which the original image suffered from low SNR introduces errors into the field map, which in turn translate to noise in the corrected image.

These examples suggest that the PSF is less sensitive to noise than the field mapping approach, and that it provides better performance in two key regions: edges, where partial volume effects may corrupt the field map; and low-intensity regions, where determination of the field map is more difficult. The images corrected using the PSF also have a better SNR than those corrected using the field map approach. These results are quantified in Table 1. The values in the table represent the pixel deviation compared with conventional spin echo. For both the phantom and the human data, the standard deviations (SDs) of this difference are ordered as: $\sigma_{\mathrm{EPI}} > \sigma_{\mathrm{field\ mapping}} > \sigma_{\mathrm{PSF}}$, indicating the superior performance of the PSF approach.

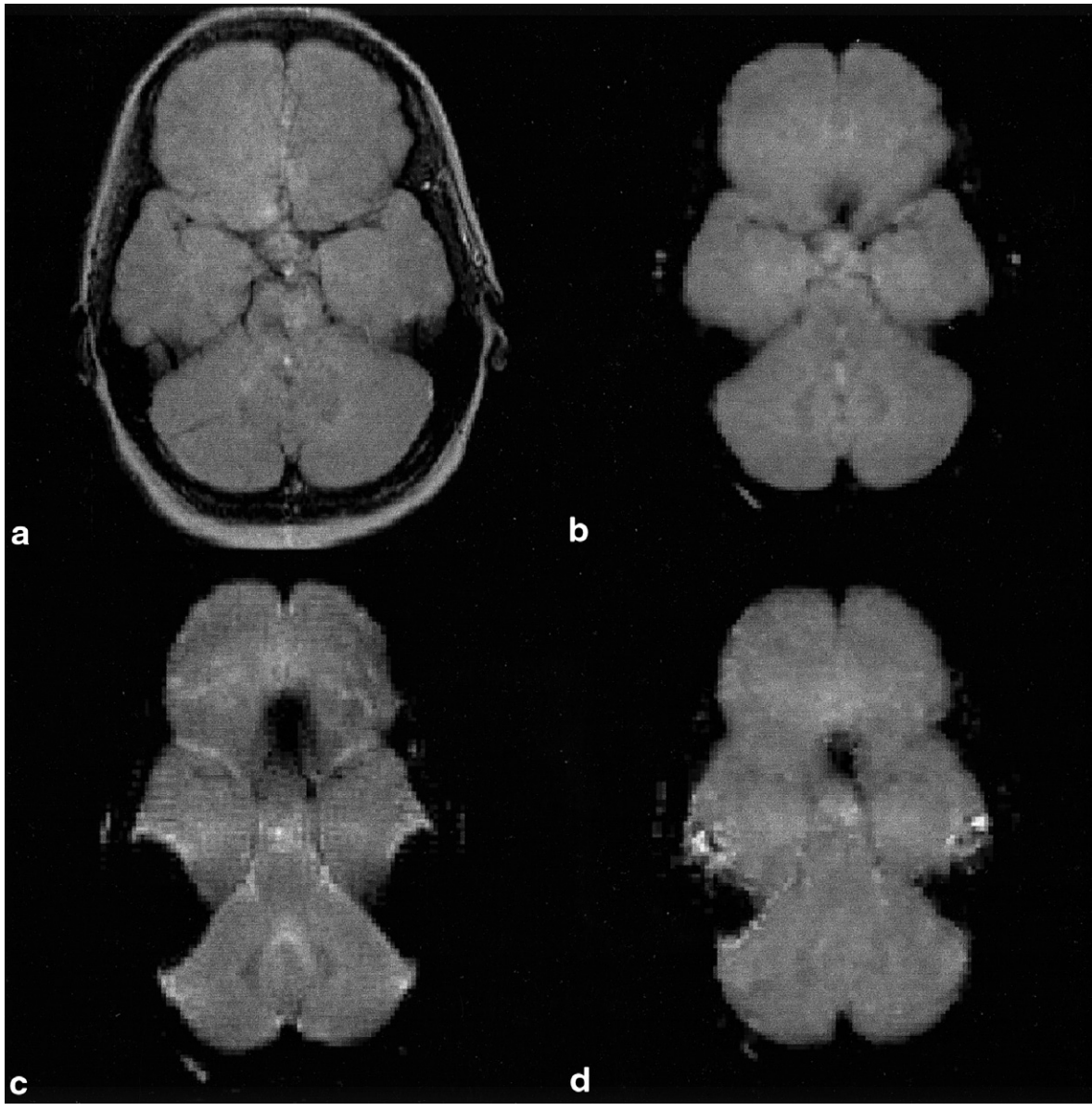

FIG. 3. Axial brain images: (**a**) conventional spin-echo image, (**b**) PSF-corrected EPI image, (**c**) uncorrected EPI image, (**d**) field map-corrected EPI image. The phase-encode direction is vertical (A/P).

To examine the impact of noise on the performance of these two methods, different amounts of noise were added to the signal in *k*-space, and the two methods were used to correct the images obtained from the signal with noise added. The results are shown in Fig. 5a and b. The abscissa represents the amount of added noise, and the *y*-axis represents the SD of the voxel-by-voxel difference between the corrected image and the reference image. The dashed line represents the PSF method, and the solid line represents results from the field mapping method. The lines with circles represent data from the phantom images, the lines with triangles are from the in vivo axial-oblique images, and the lines with squares are from the subject data obtained in the coronal plane. The results show that the PSF is less sensitive to noise across a wide range of noise levels. Noise could can be a factor in the determination of both the field map and the PSF, and it can also dominate the images to be corrected. In Fig. 5a, the noise was added to the raw data of the PSF and the field map prior to their calculation, whereas in Fig. 5b the noise was added to the images to be corrected and not to the field map or PSF raw data.

DISCUSSION

The results show that both the field mapping and PSF methods can correct geometric image distortions. The accuracy of field mapping in areas where field inhomogeneities are most severe is poor because of problems with phase wrap and signal loss in these regions. Partial volume effects (arising from fat and water in the same voxel, or different precession frequencies across a voxel due to se-

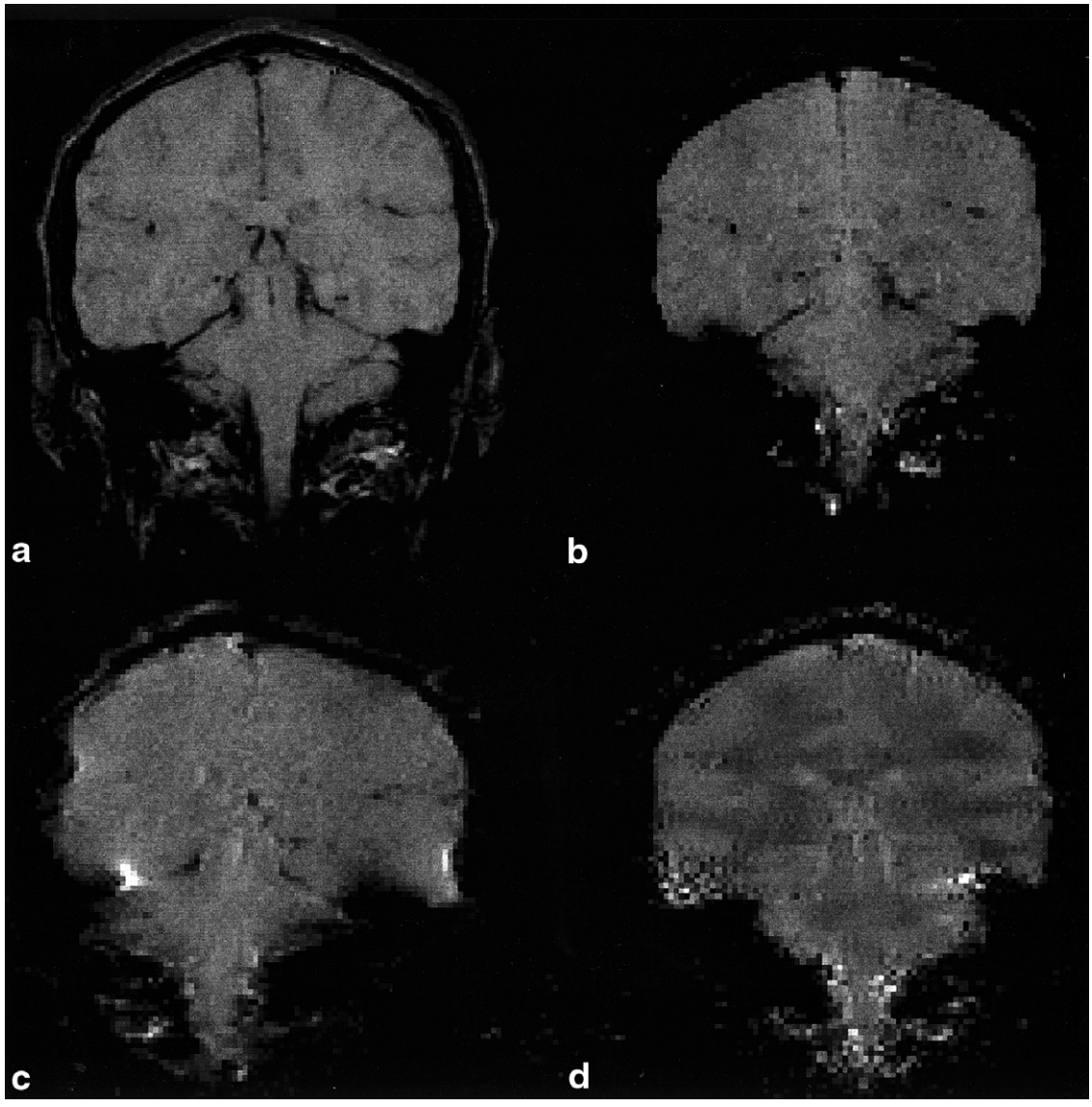

FIG. 4. Coronal brain images: (**a**) conventional spin-echo image, (**b**) image corrected using the PSF approach, (**c**) uncorrected EPI image, and (**d**) image corrected using field mapping. The phase-encode direction is horizontal (L/R).

vere field inhomogeneity) can also play a significant role in distorting the phase evolution with changes in TE—and hence the determination of the field by phase difference techniques. As shown in Fig. 6, the phase evolution with different echo offsets may not be linear in time if significant partial volume effects are present. The solid line represents in vivo data from a single voxel from the coronal brain scan. The dashed line shows a simulation of the phase as a function of time offset, in the presence of a large field inhomogeneity, which breaks the assumption that the phase evolves linearly with time. In this case it is difficult to measure the true field offset, and thus an erroneous distortion correction will be obtained if the field map is used. Unfortunately, this effect is most severe in regions that suffer the most image distortion. This is apparent in the in vivo examples shown in Figs. 3 and 4, in which the inhomogeneity is largest near tissue/air and tissue/bone interfaces.

Table 1
Average Pixel Deviations of Uncorrected, Field Map Corrected, and PSF Corrected, EPI Images Relative to the Conventional Scan of the Same Slice

	σ_{EPI}	$\sigma_{Field\ Mapping}$	σ_{PSF}
Phantom	0.69	0.60	0.58
Subject (axial-oblique)	0.54	0.53	0.51
Subject (coronal)	0.58	0.57	0.53

In general, for the field map calculation, the error in the phase measurement can be described by the following expression: $\sigma_{phase} = 1/\mathrm{SNR}_{magnitude}$. This indicates that voxels with high SNR produce low errors in the phase measurement, whereas the error in the phase measurement is large for voxels with low SNR. Errors in the phase maps translate directly to errors in the pixel shifts, and thus noise in the phase maps leads to noise in the unwarping

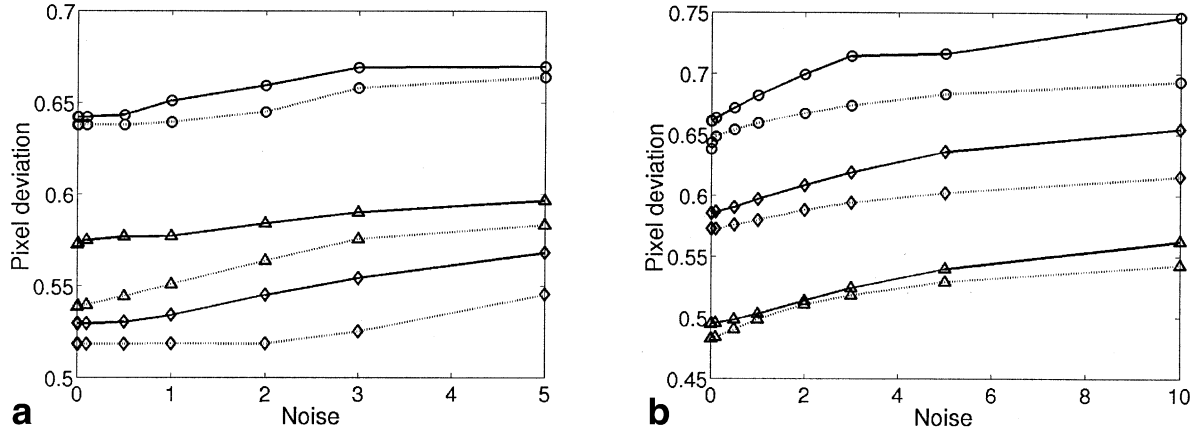

FIG. 5. **a:** Voxel-based average pixel SD between the conventional image (reference) and corrected EPI images, as a function of the level of noise added (in SDs, Gaussian distributed white noise) to the PSF and field map data. The dashed line represents images corrected using the PSF approach; the solid line is for the images corrected using field mapping. **b:** The average pixel SD between the corrected images (PSF approach, dashed line) and field map approach (solid line) and the conventional spin-echo images, as a function of noise added to the distorted images to be corrected. In both parts the data are from phantom images (circles), axial brain images (diamonds), and coronal brain images (triangles). In both cases, when (**a**) the noise was added to the PSF and the field maps, and (**b**) when the noise was added to the images to be unwarped, the PSF correction more closely matched the reference image.

when the field map method is used. Since the PSF approach does not use phase map data but integrates across all of the phase-encoding steps, it does not exhibit this low-SNR sensitivity problem. This partially explains why the low-intensity regions in the images corrected using the PSF are sharper than those corrected using field mapping.

Second, the field map $\Delta B(\vec{r})$ obtained using EPI is in the distorted space rather than the preferable undistorted space ($\Delta B(\vec{r})$). These two field maps are not the same. With the position shift $\vec{r}' = \vec{r} + \vec{a}\Delta B(\vec{r})$ as shown above, the right correction should be $\vec{r} = \vec{r}' + \vec{a}\Delta B(\vec{r})$, but using the field map in the distorted space the actual correction made is $\vec{r} = \vec{r}' + \vec{a}\Delta B(\vec{r}')$. The undistorted field map can be obtained using conventional imaging sequences, but this leads to increased imaging time and/or a decreased number of echo offsets for input into the field map calculation.

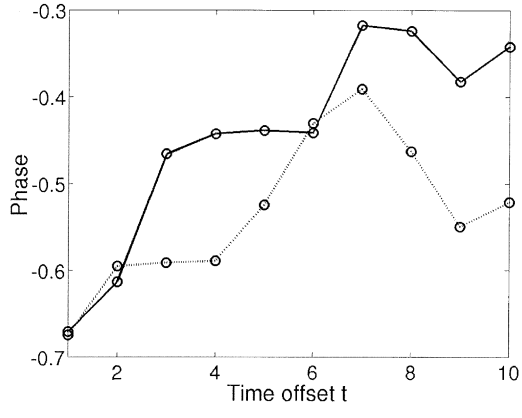

FIG. 6. Phases may not change linearly with echo offset time in the presence of a large field inhomogeneity. The phase (in radians) is shown for a given voxel in vivo as a function of time offset in the field mapping method (solid line). The dashed line shows results of a computer simulation of the phase progression with a field gradient across a voxel (ranging from 0.1–20 ppm, representing an exaggerated air/tissue boundary). Time offset is in increments of Δt = 2.5 ms.

Near tissue edges the field map distortion method encounters significant problems. Partial volume effects can lead to erroneous phase measurements at tissue boundaries, and the resultant correction of distortion is then wrong. This can be avoided by fitting a surface to the field map and extrapolating beyond the tissue boundaries. However, extrapolation is not highly precise in regions of rapidly changing field homogeneity, and if sufficient edge effects are not eliminated partial volume effects along the edges can introduce substantial errors in the underlying field maps.

Another issue to consider when correcting image distortion is the assignment of the correct image intensity to a shifted voxel. This problem is particularly important if the distortion has caused voxels to overlap. If, for example, two voxels are distorted into one voxel, or one voxel is split into two voxels, the field map approach contains no knowledge of the initial distribution of intensities in those voxels, and therefore cannot assign the correct intensity when determining the correct position of a voxel. The PSF method provides information on both the displacement and the intensity of any given voxel, and therefore can assign the correct image intensity when unwarping the image—even in the case of highly overlapping voxels.

Eddy currents caused by the fast transition of the readout gradient result in a time-varying, space-related phase shift in the data. In the field map method, the field map is determined from the phase difference of two different time offset images. If asymmetric spin-echo EPI with different offsets is used to map the field, the eddy current effects will be the same at different offsets, since the read and phase-encode gradients shift with the data acquisition. Thus the phase caused by the eddy currents is constant, and the resultant field map will not contain information about eddy currents arising from the imaging gradients.

Therefore, the field map cannot correct the distortion due to the eddy currents produced by the imaging gradients. Note that this is not the case if the sequence contains gradients for diffusion weighting—in that situation the offsets will measure different phase according to their shift relative to the applied gradients. In the PSF approach, the phase shifts caused by the eddy currents are encoded by the additional applied gradients for the PSF, so the resultant PSF contains information about the distortions arising due to both the eddy currents and local field inhomogeneities. Thus the PSF method can correct some of the distortion caused by the eddy currents. Similarly, concomitant field effects (13–15), which are primarily induced by the readout waveform (14), can add additional phase and hence distortion in the *y* direction. The PSF approach can encode the distortion caused by such fields along the phase-encode direction and thereby correct for these field effects. However, these concomitant field phase errors are independent of TE and therefore will not be encoded in the field map. Thus field mapping cannot correct concomitant gradient effects in EPI. Unlike many artifacts, such as susceptibility artifacts, the concomitant field effects decrease in severity with increasing magnetic field strength, and increase in severity with gradient strength.

Note that in the comparison between the two methods the resolution of the PSF obtained was greater than or equal to the imaging resolution, and the resolution of the field map was always equal to the imaging resolution. The PSF approach allows for the PSF to be mapped at a much higher spatial resolution (with substantial improvements in the precision of the correction) while still maintaining its ability to correct images of lower spatial resolution. The field map approach cannot be moved to higher resolutions without introducing further distortions in the field map (if they are obtained with EPI sequences), which would then be different from the distortions in the images to be corrected. However, if high-resolution field maps were obtained using conventional imaging sequences, this would introduce a registration problem, adding another level of complexity to the analysis.

In all of these comparisons the acquisition time was set to be equal for both the field map and the PSF acquisitions. It is possible to obtain a field map in much less time (only two acquisitions with different echo offsets are needed to obtain a field map), whereas the PSF can only be measured with a minimum of approximately 16 phase-encode steps in one direction. However, more acquisitions benefit the field map approach by helping to resolve the phase unwrapping problem. Since EPI is used to obtain these maps, the time penalty is quite small—even for high-resolution PSF mapping in the *y* direction. For example, if 128 phase-encoding steps are used for the PSF measurements, they could be collected in less than 1 min. In functional imaging applications wherein EPI images are collected during activation paradigms lasting 30 min to 1 hr, this short preacquisition time is minimal compared to the overall study time. The PSF approach is also susceptible to aliasing in the PSF FOV. If the chosen PSF FOV is too small, and the sampling rate is too low, the PSF can be aliased, and if undetected this could lead to significant errors in unwarping. This problem is identical to the aliasing problem in imaging.

It should also be noted that the field map method contains information on distortions in both the *x* and *y* directions, whereas, without specifically encoding in *x*, the PSF approach contains information only about distortions in the *y* direction. It is possible to collect a 2D PSF and even a 3D PSF, but, as stated in the Introduction, the imaging time increases as the power of the number of dimensions acquired. In EPI, however, the distortion in *x* is usually much smaller than in *y*, and therefore it usually suffices to correct the distortion in the phase-encode direction.

Application of the PSF approach in the slice-select direction has been used successfully to recover signal loss due to through-plane dephasing (16), and contained in that same data is information on the exact slice profile obtained in the presence of field inhomogeneities. Applying this method to both the *x* and *y* directions can provide a measure of in-plane intravoxel dephasing, and the impact of various resolution choices on signal intensity. In fact, most of the gradient shimming approaches proposed for fMRI (16–20) make use of some fraction of the complete PSF in order to compensate for field inhomogeneities, rather than correct for image distortions.

CONCLUSIONS

The comparison of the PSF method with the field map method shows that the PSF approach provides an excellent solution to the problems of geometric and intensity distortions in EPI. The field map method can be vulnerable to phase wrap, partial volume effects, and eddy current errors, while PSF is unaffected by these factors. Both techniques were tested with equivalent imaging time in order to demonstrate that with less than 1 min of prescanning, valuable information on the image distortion may be obtained. The field map approach has the advantage of providing geometric distortion information in both the readout and phase-encode directions, whereas the PSF approach can only provide this information with additional scanning. However, the PSF method can correct both intensity and geometric distortions, while the field mapping method can only correct geometric distortions. For the same acquisition time, the PSF method provides excellent information on distortion in the phase-encode direction, and has several advantages over the field mapping method. It is therefore recommended for geometric and intensity distortion correction of EPI images.

ACKNOWLEDGMENTS

The reviewers are thanked for their comments.

REFERENCES

1. Reeder SB, Faranesh AZ, Ergin A, McVeigh ER. A novel object-independent "balanced" reference scan for echo-planar imaging. J Magn Reson Imaging 1999;9:847–852.
2. Xin W, Gullberg GT, Parker DL, Zeng GL. Reduction of geometric and intensity distortions in echo-planar imaging using a multi-reference scan. Magn Reson Med 1997;37:932–944.
3. Chen NK, Wyrwicz AM. Correction for EPI distortion using multi-echo gradient echo imaging. Magn Reson Med 1999;41:1206–1213.
4. Kadah YM, Hu X. Simulated phase evolution rewinding (SPHERE): a technique for reducing B_o inhomogeneity effects in MR images. Magn Reson Med 1997;38:615–629.

5. Chiou JY, Nalcioglu O. A simple method to correct off-resonance related distortion in echo planar imaging. In: Proceedings of the 8th Annual Meeting of ISMRM, Denver, 2000. p 1711.
6. Cordes D, Arfanakis K, Haughton V, Meyerand ME. Geometric distortion correction in EPI using two images with orthogonal phase-encoding directions. In: Proceedings of the 8th Annual Meeting of ISMRM, Denver, 2000. p 1712.
7. Schneider E, Glover G. Rapid in vivo proton shimming. Magn Reson Med 1991;18:335–347.
8. Jezzard P, Balaban RS. Correction for geometric distortion in echo planar images from B_0 field variations. Magn Reson Med 1995;34:65–73.
9. Reber PJ, Wong EC, Buxton RB, Frank LR. Correction of off resonance-related distortion in echo-planar imaging using EPI-based field maps. Magn Reson Med 1998;39:328–330.
10. Robson MD, Gore JC, Constable RT. Measurement of the point spread function in MRI using constant time imaging. Magn Reson Med 1997; 38:733–740.
11. Tweig DB. The k-trajectory formulation for the NMR imaging process with applications in analysis of imaging methods. Med Phys 1983;10: 610–621.
12. Ljunggren L. A simple graphical representation of Fourier based imaging methods. J Magn Reson 1983;54:338–343.
13. Weisskoff RM, Cohen MS, Rzedzian RR. Nonaxial whole-body instant imaging. Magn Reson Med 1993;29:796–803.
14. Du YP, Zhou XJ, Bernstein MA. Correction of concomitant magnetic field-induced image artifacts in non-axial echo-planar imaging. In: Proceedings of the 6th Annual Meeting of ISMRM, Sydney, Australia, 1998. p 129.
15. King KF, Ganin A, Zhou XJ, Bernstein MA. Concomitant gradient field effects in spiral scans. Magn Reson Med 1999;41:103–112.
16. Yang QX, Williams GD, Demeure RJ, Mosher TJ, Smith MB. Removal of local field gradient artifacts in T2*-weighted images at high fields by gradient-echo slice excitation profile imaging. Magn Reson Med 1998; 39:402–409.
17. Constable RT. Functional MR imaging using gradient-echo echo-planar imaging in the presence of large static field inhomogeneities. J Magn Reson Imaging 1995;5:746–752.
18. Constable RT, Spencer DD. Composite image formation in z-shimmed functional MR imaging. Magn Reson Med 1999;42:110–117.
19. Glover GH. 3D z-shim method for reduction of susceptibility effects in BOLD fMRI. Magn Reson Med 1999;42:290–299.
20. Deichmann R, Josephs O, Hutton C, Corfield DR, Turner R. Compensation of susceptibility-induced BOLD sensitivity losses in echo-planar fMRI imaging. NeuroImage 2002;15:120–135.